

# Ballistic quantum transport through Ge/Si core/shell nanowires

D. Kotekar-Patil,<sup>1</sup> B.-M. Nguyen,<sup>2</sup> J. Yoo,<sup>3</sup> S. A. Dayeh,<sup>4,5,6</sup> and S. M. Frolov<sup>1</sup>

<sup>1</sup>*Department of Physics and Astronomy,*

*University of Pittsburgh, Pittsburgh PA, 15260, USA\**

<sup>2</sup>*Center for Integrated Nanotechnologies,*

*Los Alamos National Laboratory, Los Alamos, NM 87545, USA*

<sup>3</sup>*Center for Integrated Nanotechnologies,*

*Los Alamos National Laboratory, Los Alamos, NM 87545, USA*

<sup>4</sup>*Department of Electrical and Computer Engineering,*

*University of California, San Diego, La Jolla, CA 92037, USA*

<sup>5</sup>*Graduate Program of Materials Science and Engineering,*

*University of California, San Diego, La Jolla, CA 92037, USA*

<sup>6</sup>*Department of NanoEngineering, University of California,*

*San Diego, La Jolla, CA 92037, USA*

We study ballistic hole transport through Ge/Si core/shell nanowires at low temperatures. We observe Fabry-Pérot interference patterns as well as conductance plateaus at integer multiples of  $2e^2/h$  at zero magnetic field. Magnetic field evolution of these plateaus reveals large effective Landé g-factors. Ballistic effects are observed in nanowires with silicon shell thicknesses of 1 - 3 nm, but not in bare germanium wires. These findings inform the future development of spin and topological quantum devices which rely on ballistic subband-resolved transport.

A surge of interest in devices based on nanowires with strong spin-orbit interaction is due to their relevance for quantum computing<sup>1-7</sup> and for the realization of topological superconductivity and Majorana fermions<sup>8,9</sup>. In this context, spin-orbit interaction in germanium/silicon nanowires was predicted and estimated experimentally to be strong<sup>10-15</sup>, superconducting contacts to these nanowires were demonstrated<sup>16,17</sup>, and large Landé g-factors were reported.<sup>14,18</sup> These effects, provided they are observed in the ballistic transport regime<sup>19-21</sup>, are essential for Majorana experiments.

In this paper, we report transconductance resonances consistent with one-dimensional

(1D) subbands occupied one-by-one as the top gate voltage is made more negative. At low temperatures ( $<1$  K) transport is strongly dominated by Fabry-Pérot interference patterns. The magnetic field evolution of conductance resonances reveals large  $g$ -factors. These effects are independent of silicon shell thickness, however devices without any shell did not show ballistic transport signatures and exhibited substantial charge instabilities. We estimate the subband spacing to be  $\sim 20$  meV, the low temperature mobility of up to  $1000$   $\text{cm}^2/\text{Vs}$  and the mean free path of  $70$  nm. The mean free path is larger than the core diameter consistent with the quasiballistic regime.

Ge/Si core/shell nanowires (NWs) are grown using the low pressure, cold-walled chemical vapor deposition. NWs are grown with various core diameters ( $15 - 55$  nm) and shell thicknesses ( $0 - 4$  nm)<sup>22</sup>. Fig. 1a shows a high resolution transmission electron micrograph of a Ge/Si core/shell NW demonstrating a high degree of control over the silicon shell thickness<sup>23-25</sup>. To fabricate devices, the NWs are sonicated in isopropanol and then dropped onto  $\text{Si}_3\text{N}_4$  substrates with alignment markers. In order to achieve the low ohmic contact resistance, a dip in hydrofluoric acid is performed to etch the native oxide on the silicon shell. Electron beam evaporation and electron beam lithography are used to define two  $150$  nm thick nickel contacts. This step is followed by a  $30$  second rapid thermal annealing at  $300^\circ\text{C}$ . During annealing, Ni diffuses into the NW from both ends forming highly doped  $\text{NiGe}_x/\text{NiSi}_y$  ohmic contacts<sup>26-28</sup>. Segments of the NW between the sections of  $\text{NiGe}_x/\text{NiSi}_y$  define the Ge/Si channel length ( $L = 250 - 450$  nm). As a last step, a top gate stack consisting of a  $10$  nm thick hafnium oxide gate dielectric is deposited using atomic layer deposition and then a  $30$  nm/ $100$  nm thick Ti/Au top gate electrode is evaporated. Gate contact overlaps with the  $\text{NiGe}_x/\text{NiSi}_y$  region fully covering the unannealed Ge/Si channel. Electrical characterization is performed in a dilution refrigerator equipped with a  $9$  T magnet, using a standard lock-in technique at  $27$  Hz with an excitation voltage of  $50$   $\mu\text{V}$ . Noise attenuation is done in 2 stages: at room temperature using  $\pi$ -filters, and at low temperatures using two-stage low-pass RC filters.

Room temperature characterization of the same devices is reported by Nguyen et al.<sup>22</sup>. The room temperature saturation resistance, which is the two-terminal resistance measured at highly negative top gate voltages ( $V_g$ ), is in the range of  $10$  k $\Omega$ . The room temperature field effect mobility is  $150 - 250$   $\text{cm}^2/\text{Vs}$  for NWs with silicon shells independent of shell thickness, and  $50$   $\text{cm}^2/\text{Vs}$  for bare Ge NWs. Measurements in this work show that at low

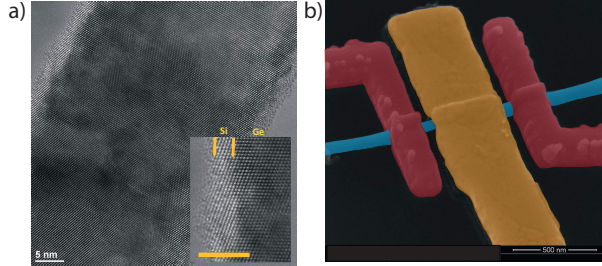


Figure 1. (a) High resolution transmission electron micrograph of a Ge/Si nanowire. Inset shows a well-defined interface between the Si shell and the Ge core. (b) False color scanning electron micrograph of a device where blue region corresponds to the NW, red regions correspond to the source and drain contacts, yellow region corresponds to the top Ti/Au gate.

temperatures the saturation resistance is comparable to the room temperature resistance (1 - 20 k $\Omega$ ). The low temperature field-effect mobility is in the range of 200 - 500 cm<sup>2</sup>/Vs with the highest mobility of 1000 cm<sup>2</sup>/Vs extracted from the pinch-off traces using gate-to-nanowire capacitance calculated by a self-consistent Poisson solver (see supplementary information).

As gate voltage is swept from positive to negative, conductance increases in steps of  $2e^2/h$  (Fig. 2a). We associate this with one-dimensional spin-degenerate subband-resolved transport. Additionally, we observe a conductance plateau below the first  $2e^2/h$  plateau. Such features are frequently reported in quantum point contacts<sup>29-32</sup> and are not the focus of this work. We further investigate this device in the non-linear regime where conductance through the NW is studied as a function of bias voltage (V) and gate voltage. Fig. 2b shows the waterfall plot in which we observe accumulations of conductance traces near  $2e^2/h$  and  $4e^2/h$ . However, plateaus at  $0.5 \times 2e^2/h$  that are expected in quantum point contacts at high bias, when the bias exceeds the subband spacing, could not be resolved due to strong current fluctuations at high bias.

Fig. 2c shows the transconductance ( $dG/dV_g$ ) of the data in the panel 2b. High transconductance resonances move linearly as a function of  $V_g$  and V. The difference in bias between points where positive and negative slope transconductance resonances meet (forming diamond-shaped regions) indicate the energy separation between the 1D subbands. From Fig. 2c, we observe that the first ( $E_{2-1}$ ) and second ( $E_{3-2}$ ) transconductance diamonds have approximately the same size of  $\approx 22$  meV. This energy separation is consistent with transverse quantization in the nanowire for heavy holes with an effective mass of  $m_{hh} = 0.28m_e$ ,

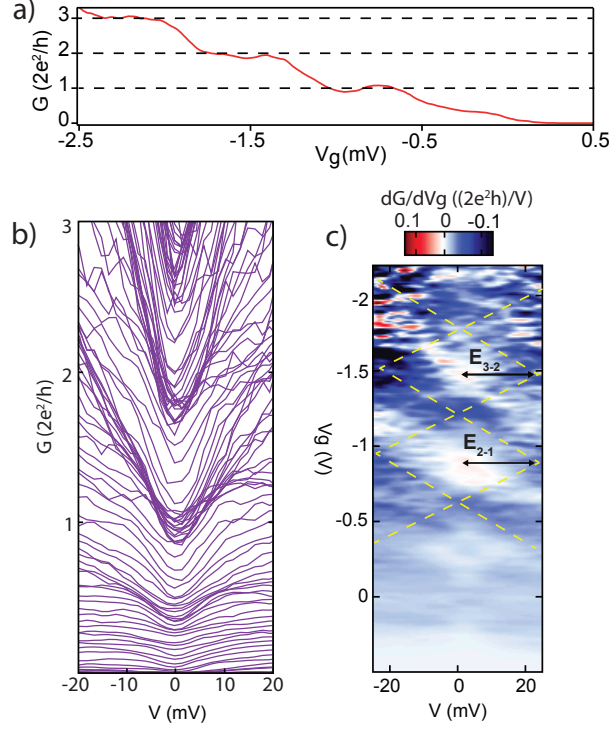


Figure 2. (a) Conductance  $G$  as a function of gate voltage  $V_g$ , at  $V = 0$  V. (b) Waterfall plot of conductance: each trace is taken at a fixed  $V_g = 0.5 - (-2.5)$  V. There is no offset between the traces. (c) Transconductance  $dG/dV_g$  of the data in panel (b) with high transconductance resonances marked by dashed lines. Energy splittings deduced from transconductance resonances are indicated by solid arrows. All data obtained at zero applied magnetic field,  $T = 5.5$  K; a series resistance of 21 k $\Omega$  is subtracted.

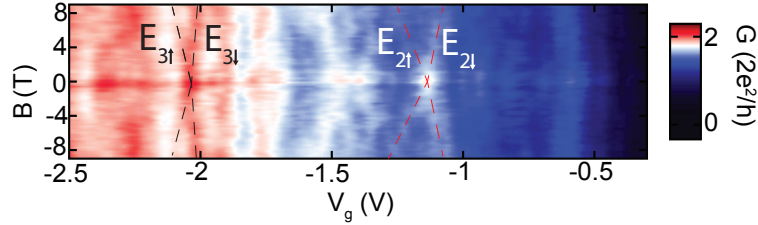


Figure 3. Differential conductance as a function of magnetic field and  $V_g$  for field oriented at an angle of  $45^\circ$  to the nanowire. Red dashed lines mark the spin split of the second conductance step ( $E_{2\downarrow}$  and  $E_{2\uparrow}$ ) and black dashed lines mark spin splitting of the third conductance step ( $E_{3\downarrow}$  and  $E_{3\uparrow}$ ).

where  $m_e$  is the free electron mass. Additionally, the slopes of the transconductance resonances are used to extract the gate lever arm parameter  $\alpha = dV/dV_g = 29.5$  meV/V.

Fig. 3 shows the evolution of conductance steps as a function of magnetic field. We note that we only observe Zeeman splitting for the second and third conductance steps. This splitting increases with magnetic field and is given by the Zeeman energy  $\Delta E_z = g \mu_B B$ ,

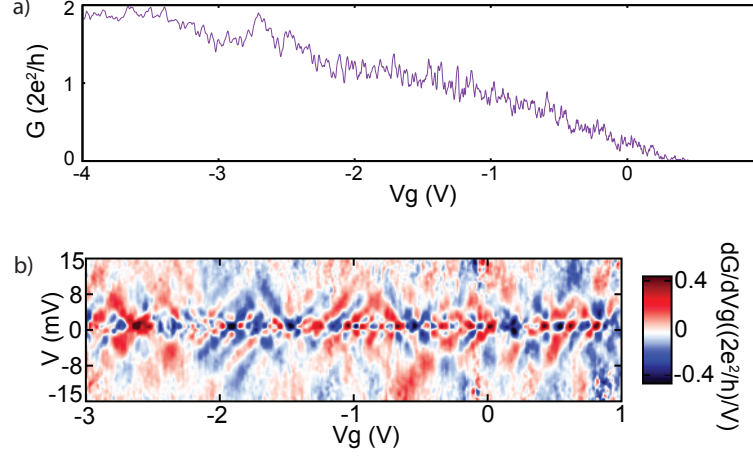


Figure 4. (a) Differential conductance at  $V = 0$  V and (b) transconductance map for a device with silicon shell thickness of 1 nm.  $T = 400$  mK,  $B = 0$  T

where  $\mu_B$  is the Bohr's magneton. We use the lever arm parameter calculated from the transconductance diamond in Fig. 2c to convert the  $V_g$  axis into the energy scale. This gives us a  $g$ -factor for each transition which we denote by  $g_2=9.6$  for transition between the first and the second conductance steps and  $g_3=5.4$  for transition between the second and the third conductance step. Large  $g$ -factors were recently observed in Ge/Si nanowire quantum dots<sup>14,18</sup>.

Fig. 4a shows a conductance trace of another device, based on a NW with diameter  $d = 35$  nm, length  $L = 350$  nm and shell thickness  $t_{si} = 1$  nm at  $T = 400$  mK. Mobility extracted from  $G(V_g)$  trace at  $T = 4$  K is  $\approx 450$  cm<sup>2</sup>/Vs. While this trace does not show conductance plateaus, it is a representative trace for many core/shell devices studied at temperatures below 1 K. With the application of negative gate voltage, conductance reaches  $4e^2/h$  indicating transport through at least two subbands. In the whole  $V_g$  range shown in Fig. 4a, conductance trace exhibits quasi-periodic oscillations. The smallest period measured in  $V_g$  is approximately  $\Delta V_g \approx 9$  mV. Fig. 4b shows the evolution of these quasi-periodic conductance oscillations as a function of  $V_g$  and  $V$ : the zero-bias features evolve into checkerboard patterns at finite bias. We attribute this to Fabry-Pérot interference<sup>21,33</sup>. The energy spacing of Fabry-Pérot resonances  $\Delta E = 1 - 2$  meV is linked to the cavity  $L_c$  length by:  $\Delta E = \frac{\hbar^2 \pi^2}{2m^* L_c^2} \approx 75\text{-}110$  nm. This implies that the segment of NW over which Fabry-Pérot interference takes place is approximately one-third of the NW channel. Using the Fermi velocity of  $10^7$  cm/s and  $\mu \approx 450$  cm<sup>2</sup>/Vs, we estimate a mean free path of  $l_s \approx 70$  nm, in good agreement with the estimate from the Fabry-Pérot resonance spacing.

To conclude, signatures compatible with conductance quantization are measured in Ge/Si NW devices. Magnetic field dependence reveals that the hole g-factor in our NWs is large and exhibits strong anisotropy. Moreover, the presence of a silicon shell on the NW results in quasiballistic transport which is absent in bare Ge NW.

### ACKNOWLEDGEMENT

The Ge/Si nanowire growth was performed at the Center for Integrated Nanotechnologies (CINT), U.S. Department of Energy, Office of Basic Energy Sciences User Facility at Los Alamos National Laboratory (Contract DE-AC52-06NA25396) and Sandia National Laboratories (Contract DE-AC04-94AL85000). We thank Z. Su for technical help and useful discussions. S.A.D. acknowledges NSF support under DMR-1503595 and ECCS-1351980. S.M.F. acknowledges NSF DMR-125296, ONR N00014-16-1-2270 and Nanoscience Foundation, Grenoble.

---

\* Current address: CEA, INAC-PHELIQS, F-38000 Grenoble, France; dharamkotekar@gmail.com

- <sup>1</sup> S. Nadj-Perge, S. M. Frolov, E. P. A. M. Bakkers, and L. P. Kouwenhoven, *Nature* **468**, 1084 (2010).
- <sup>2</sup> V. S. Pribiag, S. Nadj-Perge, S. M. Frolov, J. W. G. van den Berg, I. van Weperen, R. Plissard, M. P. A. Bakkers, and L. Kouwenhoven, *Nat Nano* **8**, 170 (2013).
- <sup>3</sup> M. Veldhorst, C. H. Yang, J. C. C. Hwang, W. Huang, J. P. Dehollain, J. T. Muhonen, S. Simmons, A. Laucht, F. E. Hudson, K. M. Itoh, A. Morello, and A. S. Dzurak, *Nature* **526**, 410 (2015).
- <sup>4</sup> D. K. Patil, A. Corna, R. Maurand, A. Crippa, A. Orlov, S. Barraud, X. Jehl, S. De Franceschi, and M. Sanquer, arXiv preprint arXiv:1606.05855 (2016).
- <sup>5</sup> R. Maurand, X. Jehl, D. K. Patil, A. Corna, H. Bohuslavskyi, R. Laviéville, L. Hutin, S. Barraud, M. Vinet, M. Sanquer, and S. De Franceschi, arXiv preprint arXiv:1605.07599 (2016).
- <sup>6</sup> H. Bohuslavskyi, D. Kotekar-Patil, R. Maurand, A. Corna, S. Barraud, L. Bourdet, L. Hutin, Y.-M. Niquet, X. Jehl, S. De Franceschi, M. Vinet, and M. Sanquer, *Applied Physics Letters*

- 109**, 193101 (2016), <http://dx.doi.org/10.1063/1.4966946>.
- <sup>7</sup> A. P. Higginbotham, T. W. Larsen, J. Yao, H. Yan, C. M. Lieber, C. M. Marcus, and F. Kuemmeth, *Nano Letters* **14**, 3582 (2014), pMID: 24797219, <http://dx.doi.org/10.1021/nl501242b>.
  - <sup>8</sup> V. Mourik, K. Zuo, S. M. Frolov, S. R. Plissard, E. P. A. M. Bakkers, and L. P. Kouwenhoven, *Science* **336**, 1003 (2012), <http://science.sciencemag.org/content/336/6084/1003.full.pdf>.
  - <sup>9</sup> S. M. Albrecht, A. P. Higginbotham, M. Madsen, F. Kuemmeth, T. S. Jespersen, J. Nygard, P. Krogstrup, and C. M. Marcus, *Nature* **531**, 206 (2016).
  - <sup>10</sup> C. Kloeffer, M. Trif, and D. Loss, *Phys. Rev. B* **84**, 195314 (2011).
  - <sup>11</sup> Y. Hu, H. O. H. Churchill, D. J. Reilly, J. Xiang, C. M. Lieber, and C. M. Marcus, *Nat Nano* **2**, 622 (2007).
  - <sup>12</sup> X.-J. Hao, T. Tu, G. Cao, C. Zhou, H.-O. Li, G.-C. Guo, W. Y. Fung, Z. Ji, G.-P. Guo, and W. Lu, *Nano Letters* **10**, 2956 (2010), pMID: 20698609, <http://dx.doi.org/10.1021/nl101181e>.
  - <sup>13</sup> M. Brauns, J. Ridderbos, A. Li, E. P. A. M. Bakkers, W. G. van der Wiel, and F. A. Zwanenburg, *Phys. Rev. B* **94**, 041411 (2016).
  - <sup>14</sup> A. Zarassi, Z. Su, J. Danon, J. Schwenderling, M. Hocevar, B.-M. Nguyen, J. Yoo, S. A. Dayeh, and S. M. Frolov, *ArXiv e-prints* (2016), arXiv:1610.04596 [cond-mat.mes-hall].
  - <sup>15</sup> F. Maier, J. Klinovaja, and D. Loss, *Phys. Rev. B* **90**, 195421 (2014).
  - <sup>16</sup> J. Xiang, VidanA., TinkhamM., W. M., and C. M. Lieber, *Nat Nano* **1**, 208 (2006).
  - <sup>17</sup> Z. Su, A. Zarassi, B.-M. Nguyen, J. Yoo, S. A. Dayeh, and S. M. Frolov, *ArXiv e-prints* (2016), arXiv:1610.03010 [cond-mat.mes-hall].
  - <sup>18</sup> M. Brauns, J. Ridderbos, A. Li, E. P. A. M. Bakkers, and F. A. Zwanenburg, *Phys. Rev. B* **93**, 121408 (2016).
  - <sup>19</sup> I. van Weperen, S. R. Plissard, E. P. A. M. Bakkers, S. M. Frolov, and L. P. Kouwenhoven, *Nano Letters* **13**, 387 (2013), pMID: 23259576, <http://dx.doi.org/10.1021/nl3035256>.
  - <sup>20</sup> W. Lu, J. Xiang, B. P. Timko, Y. Wu, and C. M. Lieber, *Proceedings of the National Academy of Sciences of the United States of America* **102**, 10046 (2005), <http://www.pnas.org/content/102/29/10046.full.pdf>.
  - <sup>21</sup> A. V. Kretinin, R. Popovitz-Biro, D. Mahalu, and H. Shtrikman, *Nano Letters* **10**, 3439 (2010), pMID: 20695446, <http://dx.doi.org/10.1021/nl101522j>.
  - <sup>22</sup> B.-M. Nguyen, Y. Taur, S. T. Picraux, and S. A. Dayeh, *Nano Letters* **14**, 585 (2014), pMID: 24382113, <http://dx.doi.org/10.1021/nl4037559>.

- <sup>23</sup> S. A. Dayeh, A. V. Gin, and S. T. Picraux, *Applied Physics Letters* **98**, 163112 (2011), <http://dx.doi.org/10.1063/1.3574537>.
- <sup>24</sup> S. A. Dayeh, N. H. Mack, J. Y. Huang, and S. T. Picraux, *Applied Physics Letters* **99**, 023102 (2011), <http://dx.doi.org/10.1063/1.3567932>.
- <sup>25</sup> S. A. Dayeh, W. Tang, F. Boioli, K. L. Kavanagh, H. Zheng, J. Wang, N. H. Mack, G. Swadener, J. Y. Huang, L. Miglio, K.-N. Tu, and S. T. Picraux, *Nano Letters* **13**, 1869 (2013), pMID: 23030346, <http://dx.doi.org/10.1021/nl3022434>.
- <sup>26</sup> Y. Wu, J. Xiang, C. Yang, W. Lu, and C. M. Lieber, *Nature* **430**, 61 (2004).
- <sup>27</sup> W. Tang, B.-M. Nguyen, R. Chen, and S. A. Dayeh, *Semiconductor Science and Technology* **29**, 054004 (2014).
- <sup>28</sup> S. Dayeh, W. Tang, B.-M. Nguyen, X. Dai, Y. Liu, Y. Hwang, X. H. Liu, and R. Chen, *ECS Transactions* **58**, 115 (2013), <http://ecst.ecsdl.org/content/58/7/115.full.pdf+html>.
- <sup>29</sup> K. J. Thomas, J. T. Nicholls, M. Y. Simmons, M. Pepper, D. R. Mace, and D. A. Ritchie, *Phys. Rev. Lett.* **77**, 135 (1996).
- <sup>30</sup> S. M. Cronenwett, H. J. Lynch, D. Goldhaber-Gordon, L. P. Kouwenhoven, C. M. Marcus, K. Hirose, N. S. Wingreen, and V. Umansky, *Phys. Rev. Lett.* **88**, 226805 (2002).
- <sup>31</sup> D. J. Reilly, T. M. Buehler, J. L. O'Brien, A. R. Hamilton, A. S. Dzurak, R. G. Clark, B. E. Kane, L. N. Pfeiffer, and K. W. West, *Phys. Rev. Lett.* **89**, 246801 (2002).
- <sup>32</sup> Y. Komijani, M. Csontos, I. Shorubalko, T. Ihn, K. Ensslin, Y. Meir, D. Reuter, and A. D. Wieck, *EPL (Europhysics Letters)* **91**, 67010 (2010).
- <sup>33</sup> M. J. Biercuk, N. Mason, J. Martin, A. Yacoby, and C. M. Marcus, *Phys. Rev. Lett.* **94**, 026801 (2005).



**SUPPLEMENTARY INFORMATION: BALLISTIC QUANTUM TRANSPORT  
THROUGH GE/SI CORE/SHELL NANOWIRES**

## Contents

Figure S1. QPC signatures in another device

Figure S2. Magnetic field evolution of Fabry-Pérot interference patterns

Figure S3. Mobility fit

Figure S4. Fabry-Pérot interference in another device

Figure S5. Low temperature transport through bare Ge NW

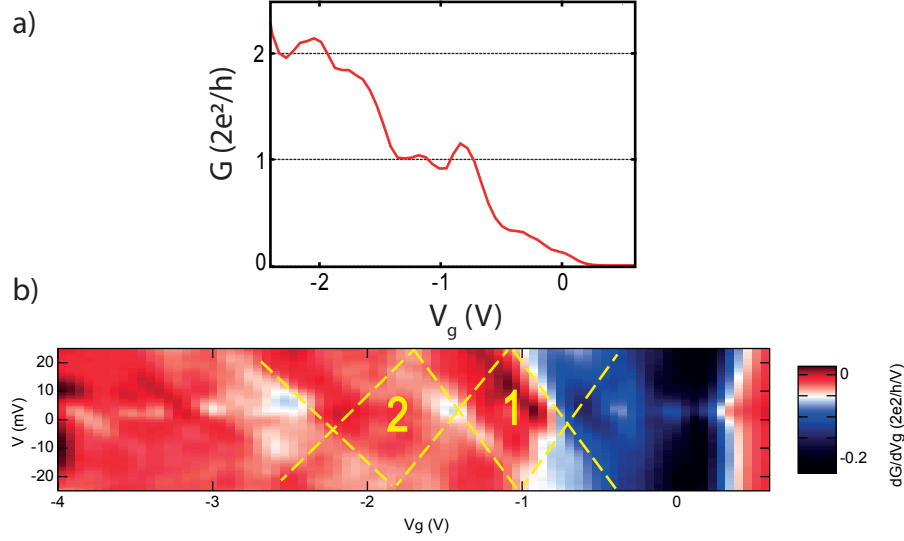


Figure 5. QPC signatures in another device (a)  $G(V_g)$  trace measured at  $T = 3.5$  K and  $V = 0$  V. NW used in this device has dimensions of  $d = 29$  nm,  $t_{si} = 3$  nm,  $L = 325$  nm. Series resistance of  $\approx 31$   $K\Omega$  is subtracted. (b) Transconductance ( $dG/dV_g$ ) of the same device as in Fig. S1a at  $T = 3.5$  K which shows conductance plateaus (marked by 1 and 2) consistent with conductance steps at zero bias. Diamond shaped regions defined in the  $V - V_g$  plane containing the conductance plateaus are marked by dashed yellow lines for the first two plateaus. The size of the diamond region is  $\approx 25$  meV in bias.

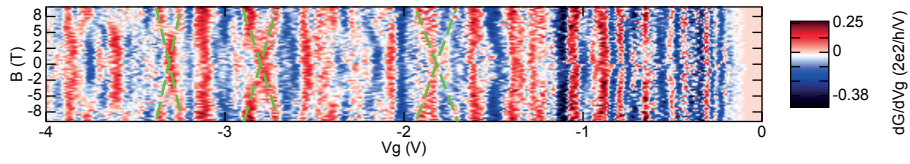


Figure 6. Transconductance  $dG/dV$  measurement of another NW device with  $d = 29$  nm,  $t_{si} = 3$  nm and  $L = 365$  nm as a function of magnetic field and  $V_g$  at  $T = 3.4$  K.  $g$ -factor extracted from the evolution of these conductance resonances are  $g = 4.9$ ,  $5$  and  $2.4$  for the green dashed lines marked from right to left. The  $g$ -factors measured in this device are consistent with the ones measured in fig. 3a of main text. However, the alignment of the magnetic field is not known.

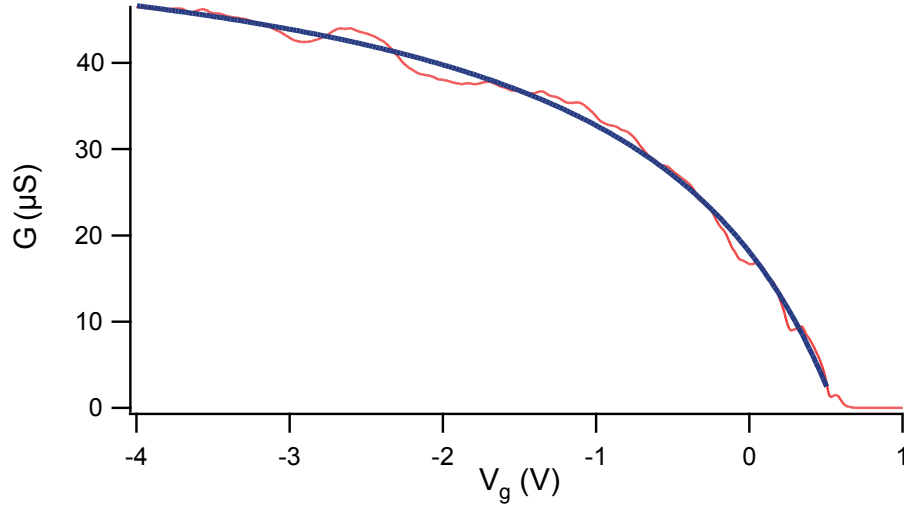


Figure 7.  $G(V_g)$  at  $T = 4\text{K}$ . Data for the same device at  $T = 400\text{ mK}$  is shown in fig. 4a of main text. Mobility is extracted using the fit equation (blue trace):  $G(V_g) = 1/(L^2/\mu C_g (V_g - V_t) + R_c)$ , where  $R_c$  is the contact resistance,  $C_g$  is the gate capacitance (evaluated using self-consistent Poisson solver) and  $V_t$  is the threshold voltage. The fitting parameters  $R_c \approx 7.5\text{ k}\Omega$  and  $\mu \approx 450\text{ cm}^2/\text{Vs}$ .

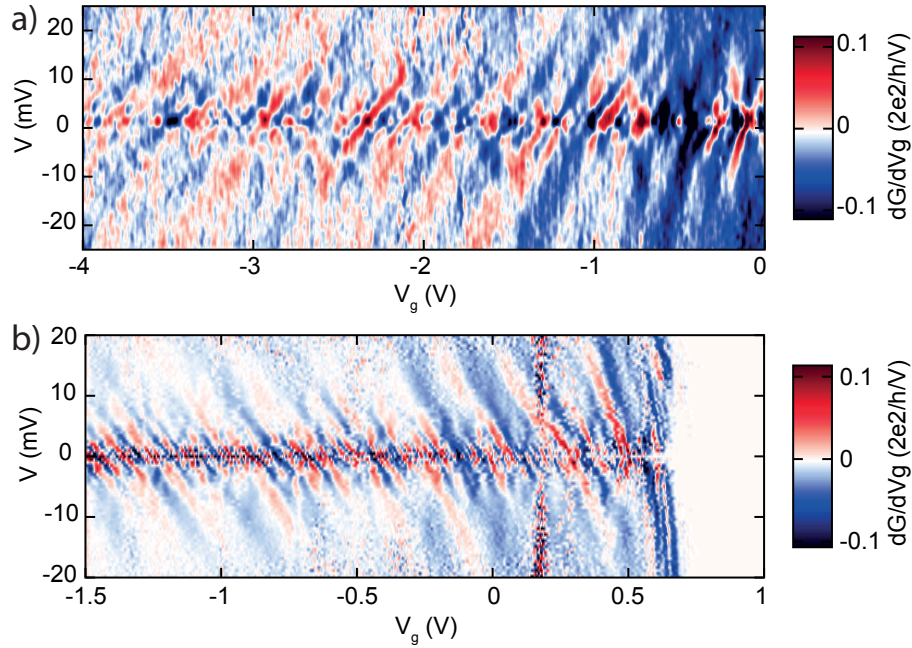


Figure 8. Fabry-Pérot interference in other devices (a) Transconductance for a device measured at  $T = 400\text{ mK}$  with  $d = 44\text{ nm}$ ,  $t_{si} = 3\text{ nm}$  and  $L = 350\text{ nm}$ . (b) Transconductance for another device measured at  $T = 30\text{ mK}$ ,  $d = 20\text{ nm}$ ,  $t_{si} = 3\text{ nm}$  and  $L = 265\text{ nm}$ . Fabry-Pérot interference is visible in both devices. Data in panel (a) and (b) are representative for all other NW devices with any silicon shell. Periodicity of the Fabry-Pérot interference is comparable to the data shown in fig. 4b of the main text.

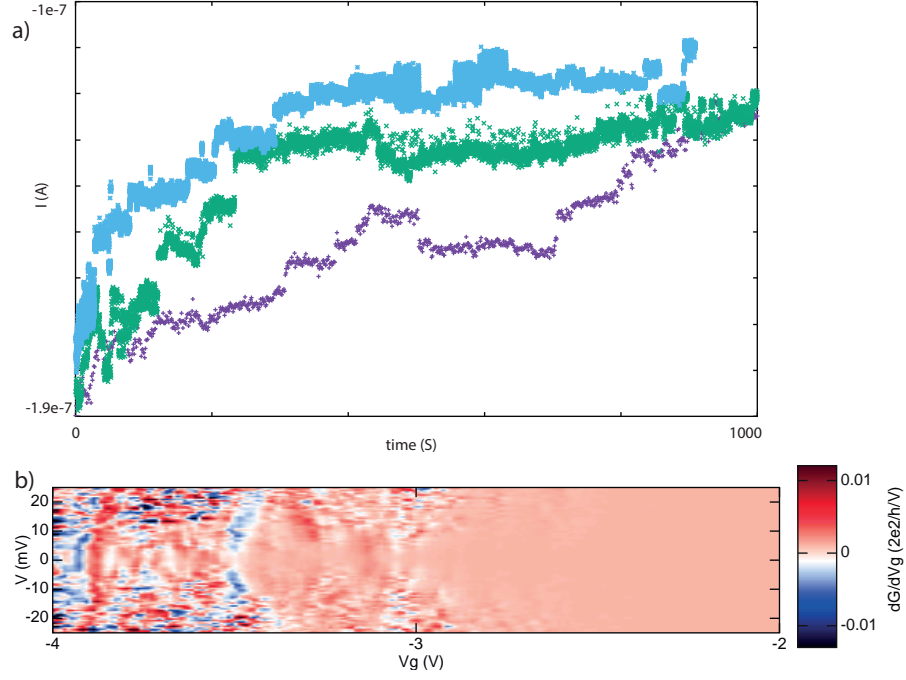


Figure 9. Transport through bare Ge NW (a) current ( $I$ ) at fixed  $V_g$  as a function of time. These data show charging and hysteresis effects that are significantly suppressed by adding a Si shell. (b) Transconductance through a device with bare germanium NW at  $T = 3.4$  K. Transport is dominated by disorder and charge instabilities.